A new in-situ peeling test for the characterisation of composite bonded joints

J. Cañas[a], L. Távara[a,*], A. Blázquez[a], A. Estefani[a], G. Santacruz[b]

[a]*Grupo de Elasticidad y Resistencia de Materiales,*
Escuela Técnica Superior de Ingeniería, Universidad de Sevilla,
Camino de los Descubrimientos s/n, 41092 Sevilla, Spain
[b]*Airbus Operations SL Getafe, Madrid, Spain*

Abstract

At the moment, bonded joints quality on composites used in aeronautical industry is verified based on the determination of the interlaminar fracture toughness (G_c) obtained by means of the Double Cantilever Beam (DCB) or the Climbing Drum Peel (CDP) tests. Although they are well-established tests, they have known limitations. This investigation presents the design and validation of a new device that carries out a peeling test, its main advantage being the capability to perform the test in-situ, i.e. directly on the actual aircraft production line without the necessity to extract coupons for a laboratory test. An experimental campaign has been carried out, the obtained results being comparable to those obtained with the traditional DCB and CDP procedures. Numerical studies have allowed to understand the delamination mechanisms presented at the different tests, confirming that experimental G_c evaluation obtained is adequate.

Keywords: Interlaminar fracture toughness, DCB, Climbing drum peel, in-situ test

*Corresponding author. Tel.: +34 954487299; fax: +34 954461637.
Email address: `ltavara@us.es` (L. Távara)

1. Introduction

The evaluation of composite-composite bonded joints quality is a major problem for the industry, in particular for the aerospace sector where the use of composite materials in primary structures has considerably increased. Given by the fact that a defective joint not only could paralyze the productive process, but it could also involve very high repairing costs. Experimental tests and numerical tools have been implemented in order to understand the failure modes and critical loads in this kind of component/structures [1, 2, 3].

A very common aeronautical structural components are the stiffened panels which include a skin reinforced by the addition of a set of stringers which are usually bonded. The main advantages of bonded joints against bolted joints are the relevant reduction of production time and that holes and other disruptions are avoided. On the contrary, the quality of the bonded joint can not be guaranteed by usual non-destructive tests (NDTs). This kind of tests are only able to determine if a large discontinuity (interface crack) between the adherent parts exists, but they are not capable to guarantee the conditions of these bonded joints. Thus, a quality control of the bonding process are demanded for Certification Authorities. Then, a test that should be able to evaluate the quality of the resulting joint of the whole process is necessary. The results of the test will capture any deficiency derived from: store conditions of the materials before the process itself, the use of an inadequate combination adherent-adhesive, the presence of pollutant agents within the bonded joint, among others.

Currently, the quality of a bonded joint in aeronautical industry is quantified by interlaminar fracture toughness (G_c) tests. The most commonly used are the Double Cantilever Beam (DCB) [4, 5, 6, 7, 8, 9] and the Climbing Drum Peel (CDP) [10, 11] tests. These tests measure Gc in a specimen that is bonded suppositionally under the same conditions as actual parts

2

(usually taken from these components). One disadvantage on both tests is that they cannot be carried out "in-situ", i.e. on specimens over actual parts. Moreover, there are still some open questions e.g. regarding the way G_c is calculated and the actual fracture mode occurring on the tests, among others. Although DCB and CDP are the most common tests, there are some alternatives as the peel test [12] or the mandrel peel test [13] but they also have similar disadvantages.

The aim of the present investigation is to design and validate a new device able to determine G_c "in-situ", preserving the advantages of the DCB and CDP tests and also overcome some of their drawbacks.

The paper is organized as follows. The main characteristics of the currently used tests (DCB and CDP) are described in Section 2. Then, the principles for the new test are discussed in Section 3. The results for the test campaign are presented in Section 4 and the numerical results (virtual testing) are included in Section 5. Finally, Section 6 contains the conclusions of the present investigation. Some Appendices are also presented with the aim to answer some of the questions raised on the new test concept.

2. G_c tests overview

In general terms, DCB and CDP tests relies on the fracture toughness calculus defined as the released energy by area unit within an interface crack Gc, defined as:

$$G_c = \frac{\triangle E}{\triangle S} = \frac{\triangle E}{b\triangle a} \tag{1}$$

where E is the energy necessary for crack propagation as function of the load and associated displacement, S is the surface formed due to crack propagation, a is the crack length and b is the specimen width. Previous expression assumes that the crack extends across the whole width of the

3

specimen. Usually on every test configuration this asumption is correct as the crack front is regular.

In the following the main aspects of both tests are described. It is important to recall that G_c only equals G_{Ic} (fracture toughness in pure fracture mode I) under very specific loading and geometrical conditions of the specimens, as it will be discussed later on.

2.1. DCB test

The widest used test to obtain the fracture toughness is the DCB test. This test is used to determine the interlaminar fracture toughness in a composite material (i.e. between two laminaes within a laminate) [4, 6, 7] or to determine the interface fracture toughness of adhesively bonded joints (i.e. an interface crack grows along an adhesive layer) [5].

In the aeronautical industry, usually companies use their own standards [4, 5]. These standards use the load - displacement plot, obtained during the test, to calculate the fracture toughness using:

$$G_c = \frac{A}{ba} \tag{2}$$

where A is the area of the pseudo-triangle defined by the origin and the load- displacement plot between two points, b is the specimen width and a is the increment of the crack length between the chosen points (usually 60 mm).

Nowadays, DCB is the reference test to evaluate G_c. Its main advantages includes: (i) it is able to determine the fracture toughness in pure mode I ($G_c = G_{Ic}$) when symmetrical configurations are used, (ii) it is easy to perform, moreover expensive tooling is not necessary. Nevertheless, it also has some disadvantages: (i) standards require to measure the crack length which is not always an easy task, (ii) for thin laminates (when finite displacements appear) G_c formulae in the standards are not adequate even

4

using the correction factors included there [14], (iii) when non-symmetrical laminates are used the way fracture toughness is calculated is not adequate due to $G_c \neq G_{Ic}$ [15, 16] , (iv) it is not possible to perform the test "in-situ".

2.2. CDP test

An alternative to the DCB test is the so-called Climbing Drum Peel (CDP) test [11]. This test was originally conceived to evaluate the bonded joints between a flexible adherent and a rigid adherent or between the skin (laminate) and the core in a sandwich panel [10]. The test consists in winding a flexible laminate (which peels at the same time it winds) using a drum with two different radii ($r_2 > r_1$). The laminate is fixed to the drum in its central part which has radius r_1. The outer parts (borders) of the drum (with larger radius, r_2) includes two loading straps which will apply the torque required for the drum progression along the specimen. The ends of the loading straps are fixed at the bottom of a universal testing machine, while the un-cracked end of the specimen is attached to the upper jaws of the machine. Once the specimen is collocated, the upper cross-head of the machine moves up provoking that the flexible laminate gets into contact (winds) with the inner part of the drum. Then, the drum "climbs" along the specimen propagating the initial pre-cracked zone while the flexible laminates winds. A scheme of the test can be found in [11].

In the load-displacements plots obtained during the tests, two constant load levels can be clearly observed. One associated to the winding load (F_w) and the other one associated to the winding+delamination process (F_d). Usually, F_w is calculated on a second stage of the test once a very large pre-cracked zone is presented. Then, the fracture toughness is evaluated using (3).

$$G_c = \frac{(F_d - F_w)(r_2 - r_1)}{br_1},\qquad(3)$$

5

where b is the width of the specimen.

It is remarkable that the configuration of the test and the imposed kinematics leads to a stable crack propagation, under a constant applied force. Then, G_c calculation is straightforward as it is proportional to the constant applied force. Moreover, the crack growth is directly related to the applied displacement during the test. This fact implies that it is not necessary to measure the crack length. On the other hand, it is clear that the obtained fracture toughness with this test is not associated to pure fracture mode I ($G_c \neq G_{Ic}$), thick laminates ($> 1mm$) could not be tested (undesirable break of the laminate may occur) and finally, the test can not be performed "in-situ".

3. Horizontal Drum Peel (HDP) test

As described in the previous section, both DCB and CDP tests use a universal testing machine to apply the load. This fact makes impractical to perform these tests "in-situ". The aim of the present investigation is to design a new test configuration with the following characteristics: (i) no need to measure the crack length, (ii) easy to perform, (iii) straightforward Gc evaluation, and (iv) able to perform "in-situ" [17].

The initial idea was to perform a Drum Peel in a horizontal position and without the use of a universal testing machine. Thus, the rotation could be applied directly to the drum using an engine which moves a kinematic chain in order to get an adequate speed rotation. A torque cell will measure the torsional moment needed along the test.

Obtained numerical results for the simplified problem presented in the Appendices, showed that critical radius values, R_c (producing the critical moment, M_c, that causes delamination), are different for each bonding configuration. A design able to reproduce these R_c values at the crack tip would be the ideal one.

6

If the drum radius, R_D, plus half of the thin laminate thickness, $t/2$, equals R_c the laminate will touch the drum during the whole delamination process, on the contrary it will separate.

When $R_D + t/2 < R_c$ results will depend on the gripping system, then a self-similar crack propagation is not assured.

Finally, when $R_D + t/2 > R_c$ the thin laminate separates from the drum. This separation is produced as the curvature (on the thin laminate) progressively changes in order to reach its corresponding R_c value at the crack tip. Moreover, during the whole delamination process R_c remains the same, i.e. a self-similar crack propagation occurs. Due to this fact, it is unnecessary to measure the crack length during the test and, additionally, results will not be affected by this separation. That is why, this is the chosen condition.

The complete test in the chosen HDP configuration includes two parts: (i) the laminate "winds" over the drum and (ii) after increasing the applied torque in the drum, "'winding+debonding" occurs. It is important to notice that the bending moment occurring in the section of the thin laminate which is over the crack tip (M) is the only responsible of the crack growth. Thus, when this moment is lower than the critical one debonding will not occur. Two stages occurring after "winding only" part of the test can be identified:

1. Initially, the separation of the laminate from the drum increases while M increases too. Once M reaches a certain value, M_c, the crack starts to propagate while the laminate also increases the separation from the drum.

2. After a while, the separation of the drum remains constant, leading to a self-similar crack growth i.e. the crack advance is equal to the winding in the upper part of the drum.

On Figure 1, the present Horizontal Drum Peel (HDP) concept is shown. Notice that, the thick laminate is fixed at the bottom and the thin laminate is clamped to the drum in one of its extremes. A torque is imposed at the
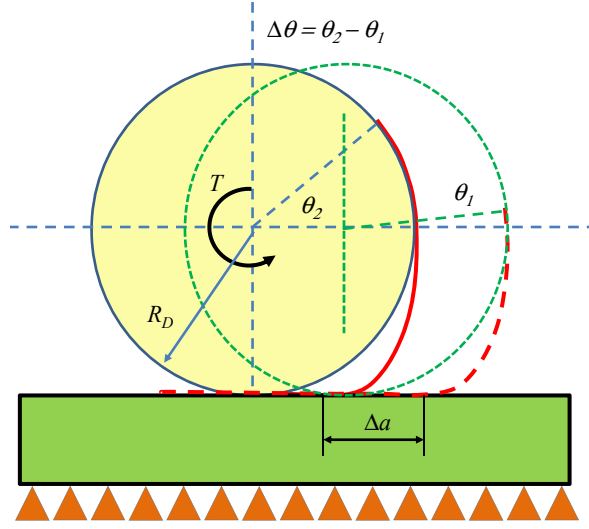
7

Figure 1: Scheme of the HDP concept.

centre of the drum while it is free to move both horizontally and vertically. During the delamination process the crack length increment, $\triangle a$, and the applied increment of rotation of the drum, $\triangle \theta$, are related by:

$$\triangle a = R_L \triangle \theta, \text{ with } R_L = R_D + \frac{t}{2} \qquad (4)$$

It is important to note that, during this stage, M_c remains constant and it is directly related to R_c, in the section over the crak tip. Moreover, although the curvature changes on the part where the laminate separates, the moments produced in any other section of the laminate do not affect the crack advance. Although, R_c can not be controlled, it can be calculated as it is function of the laminate properties and the adhesive used, see Appendix A. This fact is confirmed by the numerical analysis done in Section 5.

An energetic balance and expression (4) allows to compute $\triangle E$:

$$\triangle E = (T_d - T_w)\triangle \theta, \qquad (5)$$

where T_d and T_w are the moments (torque) associated to the wind-

ing+delamination process and only winding process, respectively. Finally, G_c can be obtained using:

$$G_c = \frac{(T_d - T_w)}{bR_L},\qquad(6)$$

where b is the width specimen.

In order to prove HDP results validity, a test campaign and a virtual testing was done in the present investigation. Moreover, CDP tests are also performed for comparison purposes.

4. Experimental tests campaign

Two bonding configurations were used for the campaign with two options for the thin laminate: Unidirectional 2 with $t = 0.5$ mm (tape) and Woven fabric [+45/-45] with $t = 0.75$ mm (fabric), see Tables 3 and 4 for the laminate and bonding configuration properties.

Manufacturing of every coupon follows a co-bonding procedure. First, the thick laminate is cured using common procedures but leaving the peel-ply on one side. After this curing cycle, the peel-ply is removed and the thin laminate is joined to the thick laminate using an adhesive layer over the surface where the peel ply has been removed. The pre-crack is obtained by including a teflon film in the desired zone. Then, the whole system is subjected to a curing cycle, where both the thin laminate and the adhesive are cured at the same time. The materials used are: Adhesive: FM 300.k05, Tape: M21E35%/UD194/T800S-24k and Fabric: GM926+RTM6.

The CDP tests were performed following [10]. A drum made of steel with inner radius $r_1 = 75$ mm and outer radius $r_2 = 95$ mm is used. Two steel loading straps with 0.2 mm in thickness and 25 mm in width, complete the tooling of the test. The total weight of the tooling was 25.5N. In figure 2, the set-up of the test is shown. Five coupons were tested for each configuration (tape or fabric).

9

Figure 2: CDP test experimental set-up.

As described in Section 2.2, the winding load (F_w) and the force associated to the winding+delamination process (F_d) are used to calculate the G_c value, see (3). The obtained experimental curves are shown in Figure 3. The dispersion obtained for the different coupons are acceptable. Nevertheless, It should be noted that the scattering is higher when the thin laminate is made of a woven fabric. It may be caused by two reasons: (i) the weave pattern in the fabric, and (ii) different failure mechanisms observed for the tape and fabric case. On the one hand, a debonding (failure of the adhesive) mostly occur when the tape is used on the thin laminates. On the other hand, stitching (detach of fibres) also occur on fabric coupons, see Figure 7.

As mentioned previously, two clear constant force zones are obtained. Then, F_d and F_w values are obtained by averaging the forces along those
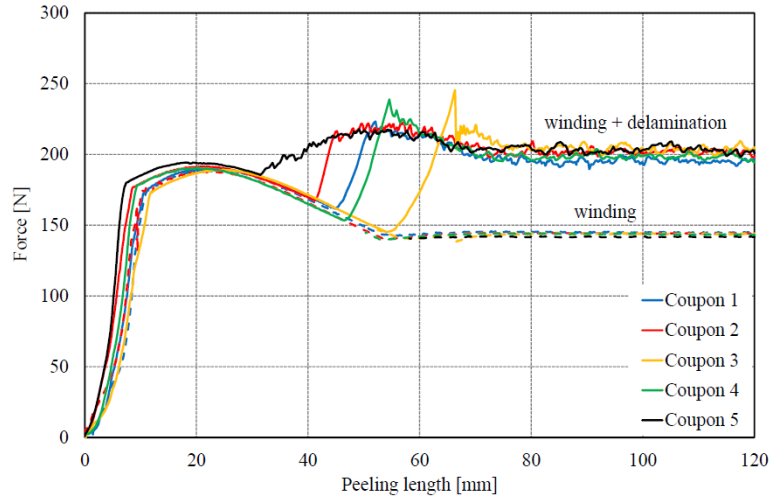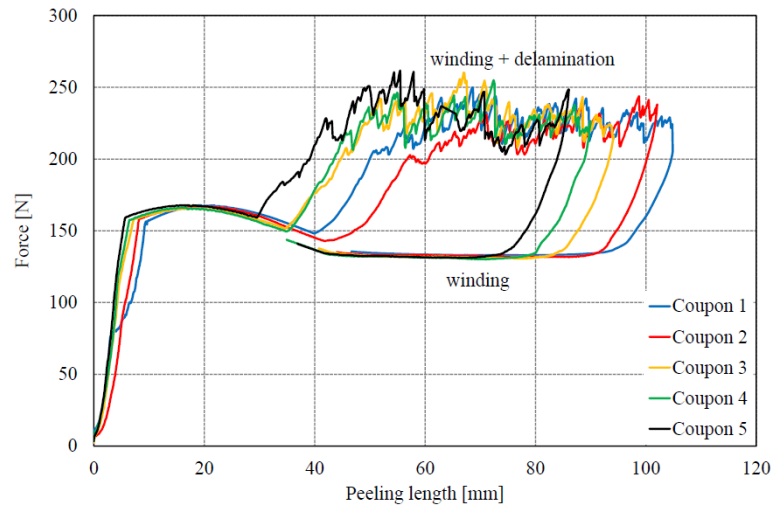
Figure 3: Experimental results obtained using the Climbing Drum Peel test for (a) tape and (b) fabric.

quasi-constant zones. Moreover, F_d and F_w can be measured by a two stage test procedure, i.e. the test is done twice the first time winding+delamination is produced while the second time only winding occurs, see Figure 3(a). The other option is to measure F_d and F_w using a single stage test procedure, i.e. the force is recorded during loading (while winding+delamination is

11

produced) and also during the unloading part of test (where only unwinding is produced), see Figure 3(b). Both procedures have shown to produce same results.
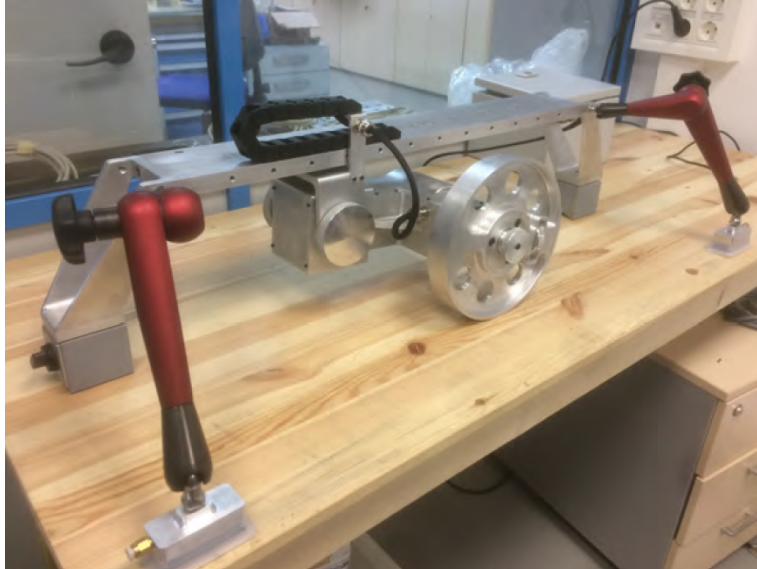

Figure 4: CDP test experimental set-up.

Regarding the new HDP test, the chosen drum radius is 95 mm and it is made of aluminium. The rotation of the drum is induced by an engine that moves a kinematic chain which is able to produce the adequate rotation velocity of the drum. A torsion loading cell measures the applied torque for the drum rotation. The torque values are recorded during the winding+delamination process, T_d, and the only winding process, T_w. The whole system is mounted over a structure so that the drum is free to move both horizontally and vertically. In Figure 4, the HDP prototype is shown. The equipment is fully autonomous and it can be fixed to any surface through suction cups located at its bottom part. The elevation of the drum can be regulated for an easier handle when irregularities and obstacles may be found in the vicinity of the thin laminate. A Lab-View control software is used for data process.

12
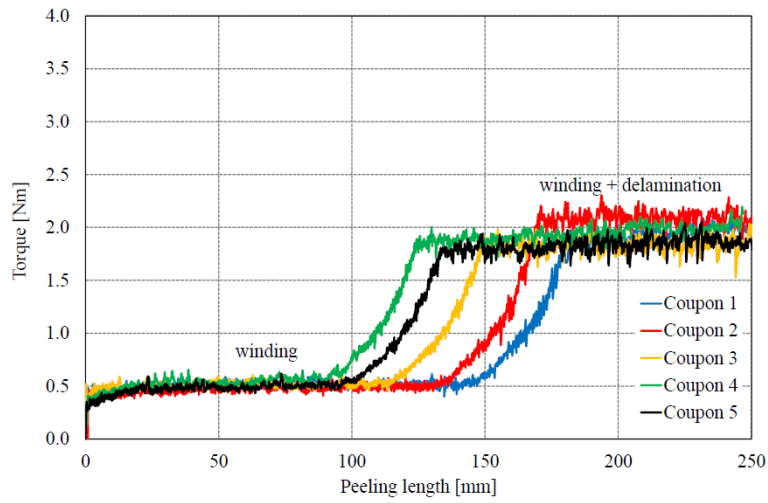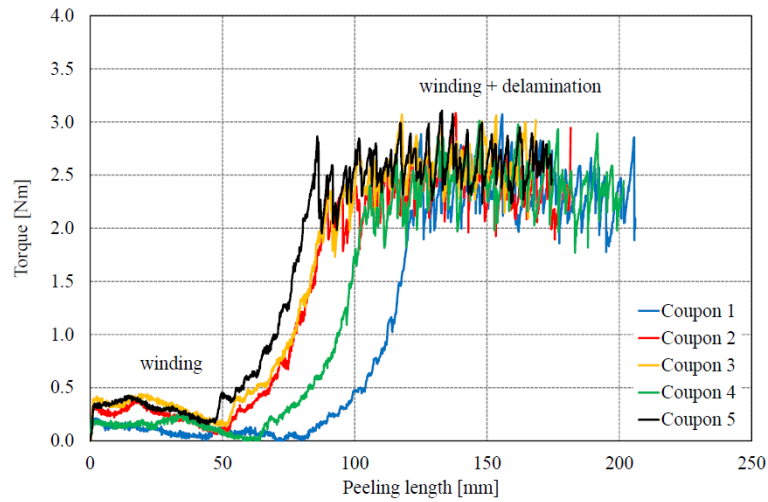
Figure 5: Experimental results obtained using the Climbing Drum Peel test for (a) tape and (b) fabric.

The coupons for the HDP test include a thin laminate bonded to a thick laminate which has no limitations on dimensions as it is thought to be much larger in an "in-situ" case. Regarding the thin laminate, it is 25 mm in width, a small thickness, t, and at least 250 mm in length, where 100 mm will be a pre-cracked zone and 150 mm will be bonded. These dimensions

were chosen in order to be able to obtain T_d and T_w values in a test with a single stage. Thus, T_w will be obtained at the initial part of the test (only winding is produced) and T_d will be measured on the second part of the test.

Anew, five coupons were tested for each configuration (tape or fabric). In Figure 5, HDP experimental curves are presented. It should be noted that the dispersion obtained are acceptable, due to the small obtained torque values, once again a higher scattering is obtained for the fabric case.

(a)

(b)
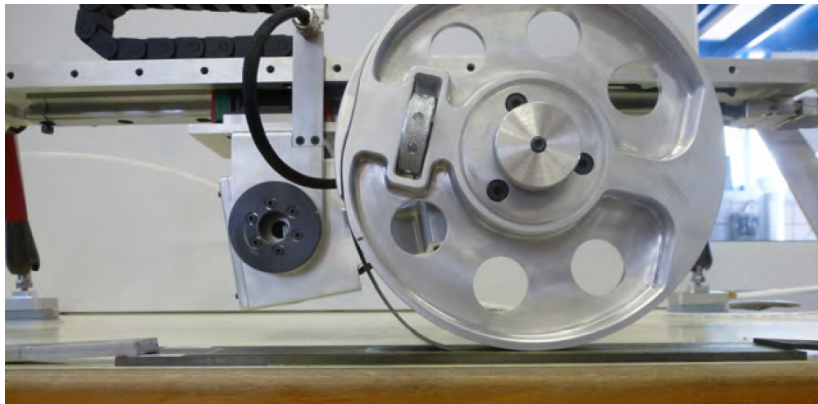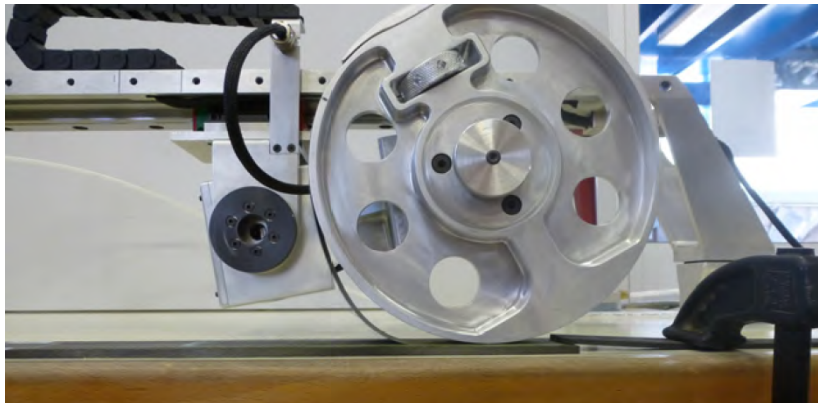
Figure 6: Separation of the thin laminate during the winding+delamination process in the HDP test at two different moments.

It is interesting to note that during the whole CDP test the thin lam-

14

inates did not present any visible separation from the drum. This fact is associated to the axial force on the thin laminated derived from the load and the drum weight. On the other hand, on the first stage of the HDP test (winding only) the thin laminate curvature follows the drum radius, but on the second stage (delamination+winding) it separates from the drum, see Figure 6. This was an expected behaviour as the thin laminate tends to a curvature equal to its corresponding critical radius (R_c), as explained in Appendix A. Nevertheless, this separation remains constant leading to a self-similar crack growth during this part of the test.

Table 1: CDP and HDP tests characteristics and G_c results for the tape.

Coupon	Climbing Drum Peel					Horizontal Drum Peel				
	b[mm]	t[mm]	F_d[N]	F_w[N]	G_c[J/m^2]	b[mm]	t[mm]	M_d[Nm]	M_w[Nm]	G_c[J/m^2]
1	25.14	0.58	198.2	145.0	557.6	25.18	0.52	1.94	0.51	598.5
2	25.27	0.60	201.3	143.8	598.3	25.18	0.53	2.09	0.48	671.6
3	25.19	0.60	206.5	143.8	654.5	25.28	0.56	1.84	0.52	549.5
4	25.18	0.58	198.5	143.1	579.2	25.18	0.56	1.97	0.54	598.5
5	25.15	0.55	203.1	141.7	642.8	25.34	0.55	1.86	0.49	568.5

In Table 1, the main results obtained from the CDP and the HDP tests for the tape case are summarized. G_c values for both tests are calculated using (3) and (6), respectively. The average of the obtained G_c values using CDP is 606.5 J/m^2 while using HDP is 597.3 J/m^2. Concluding that G_c values obtained using CDP and HDP are very similar.

In Table 2, CDP and HDP results for the fabric case are summarized. The average of the obtained G_c values using CDP is 932.6 J/m^2 while using HDP is 952.6 J/m^2. Once again, it can be concluded that G_c values obtained using CDP and HDP are in good agreement with each other.

Regarding the obtained fracture surfaces, both CDP and HDP tests produced similar results. In Figure 7, obtained fracture surfaces for tested tape and fabric specimens using HDP are shown. The coupons made of tape show a debonding mechanism i.e. failure of the adhesive. The coupons made of

15

Table 2: CDP and HDP tests characteristics and G_c results for the fabric.

		Climbing Drum Peel				Horizontal Drum Peel				
Coupon	b[mm]	t[mm]	F_d[N]	F_w[N]	$G_c[\text{J/m}^2]$	b[mm]	t[mm]	M_d[Nm]	M_w[Nm]	$G_c[\text{J/m}^2]$
1	25.14	0.58	198.2	145.0	557.6	25.18	0.52	1.94	0.51	598.5
2	25.27	0.60	201.3	143.8	598.3	25.18	0.53	2.09	0.48	671.6
3	25.19	0.60	206.5	143.8	654.5	25.28	0.56	1.84	0.52	549.5
4	25.18	0.58	198.5	143.1	579.2	25.18	0.56	1.97	0.54	598.5
5	25.15	0.55	203.1	141.7	642.8	25.34	0.55	1.86	0.49	568.5

fabric show a debonding + stitching failure mechanism where the failure of part of the laminate occurs, i.e. some fibres are detached.

Figure 7: Fracture surfaces obtained for the fabric (left) and tape (right) case in the HDP test.

5. Virtual testing

The aim of the FEAs is to reproduce numerically the curves obtained in the experimental test campaign. These numerical results helped to understand the behaviour of the delamination during the test. Moreover, the Virtual Testing also includes numerical results for CDP tests.

5.1. FE model

The FEA includes a 2D model in the commercial code Abaqus [18]. CDP and HDP models has the following similar characteristics: (i) both laminates include orthotropic properties as described in Table 3, (ii) the drum is modelled through an analytical rigid surface with a central node that controls the displacements and rotations, (iii) non-linear geometries (finite displacements and rotations) are used in the model, (iv) contact interactions between the drum and the thin laminate and between both laminates are also included, (v) the interface between the thin and the thick laminate includes a pre-cracked zone, (vi) and finally, the adhesive behaviour is included by using Abaqus built-in cohesive elements (COH2D4) which includes a bilinear traction-separation law and the Benzeggagh-Kenane damage criterion [19], see Table 4. G_{Ic} values used are obtained from a DCB test campaign for a tape/adhesive/tape configuration and a fabric/adhesive/fabric configuration when a FM300.k05 adhesive is included. G_{IIc} values are assumed using the proportions found in [20] for the same kind of adhesive.

Table 3: Properties in material coordinate system of the laminates used for the simplified model.

Laminate	$E_{11}(GPa)$	E_{33} (GPa)	G_{12}(GPa)	ν_{12}
Unidirectional 1	182	10	5	0.3
Unidirectional 2	135	10	5	0.3
Woven fabric	66	10	4.5	0.05

Additionally to the previous common characteristics, specific boundary conditions for the HDP consider, see Figure 8(a):

- The bottom line of the thick laminate is fixed.

- The free lateral edge of the thin laminate is attached to the drum by means of a Multi-point constraint (MPC) restriction.

17

Table 4: Properties of the interface model used for both bonding configurations, $\eta = 2$ always.

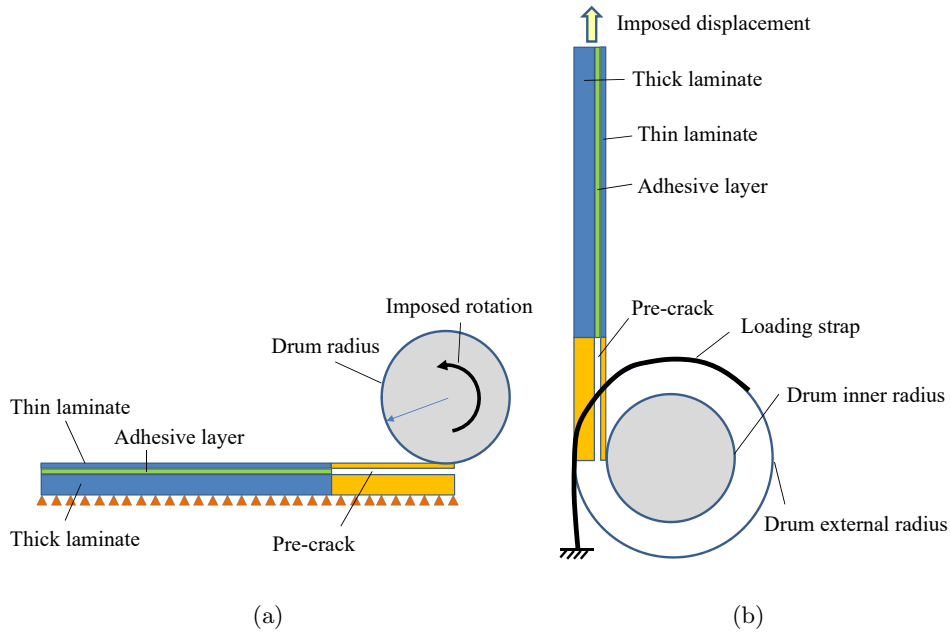| Bonding configuration	σ_c (MPa)	τ_c (MPa)	G_{Ic} (Jm^{-2})	G_{IIc} (Jm^{-2})
BC1	6	40	600	1200
BC2	6	40	870	2000

Figure 8: Boundary conditions over the (a) HDP model and (b) CDP model.

- A rotation is imposed on the central node controlling the drum, provoking the winding of the thin laminate and its subsequent delamination.

On the other hand, the FEA for the CDP test includes, see Figure 8(b):

- The extreme where the thick and the thin laminates are bonded is where the applied displacement is imposed.

18

- The drum weight is included by imposing an equivalent force in the centre of the analytical circumference, modelling the drum.

- The loading straps are also included, with 0.2 mm in thickness and 50 mm in width (modelling two straps with 25 mm in width). They are modelled using steel properties, i.e. $E = 210$ GPa and $\nu = 0.33$. The length of the straps is that corresponding to an inner radius equal to 97 mm (slightly larger than the outer CDP drum radius).

- Contact conditions are also included between the loading straps and the drum.

5.2. Experimental and numerical correlation

In this section, numerical results for the cases studied experimentally are presented and compared to them.

In Figure 9, experimental and numerical force-displacement curves for the CDP tests are presented. As can be seen, there is a very nice correlation between both results. 623.5 and 948 J/m^2 were the G_c values obtained numerically for the tape and fabric case, respectively. The experimental values being 606.5 and 932.6 J/m2 respectively, leading to a difference lower than 3% in both cases.

In Figure 10, experimental and numerical torque-displacement curves are presented. Once again, there is a very good correlation between both results. 615 and 923 J/m^2 were the G_c values obtained numerically for the tape and fabric case, respectively. The experimental values being 597.3 and 952.6 J/m^2 respectively, leading to a difference lower than 4% in both cases.

It is also interesting to observe that the deformed shape obtained for HDP numerical model is almost identical to the one obtained during the experimental tests, as can be seen in Figure 11. In that figure the green lines correspond to the numerical obtained solution which are superposed to an experimental picture.
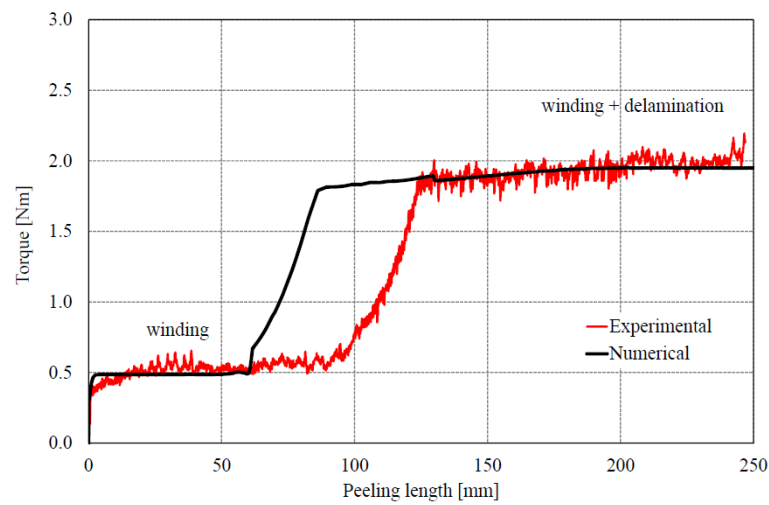
19

(a)
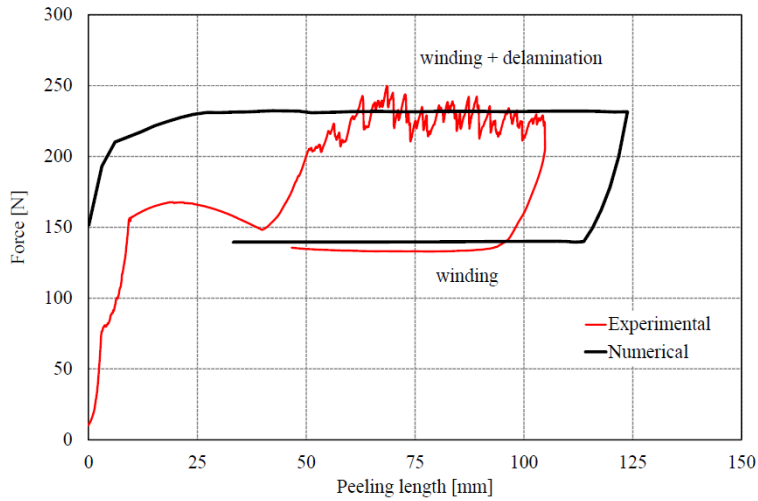
(b)

Figure 9: Numerical and experimental results obtained using the Climbing Drum Peel test for (a) tape and (b) for a fabric.

Finally, the numerical results allowed us to measure the fracture mode mixity occurring during the delamination in both CDP and HDP simulations. It is done by a post-process of the data obtained following [21], see details in Appendix B. ψ values were 9.1° and 14.6° for the CDP models (tape and fabric, respectively), while ψ were 8.2° and 13.2° for HDP models
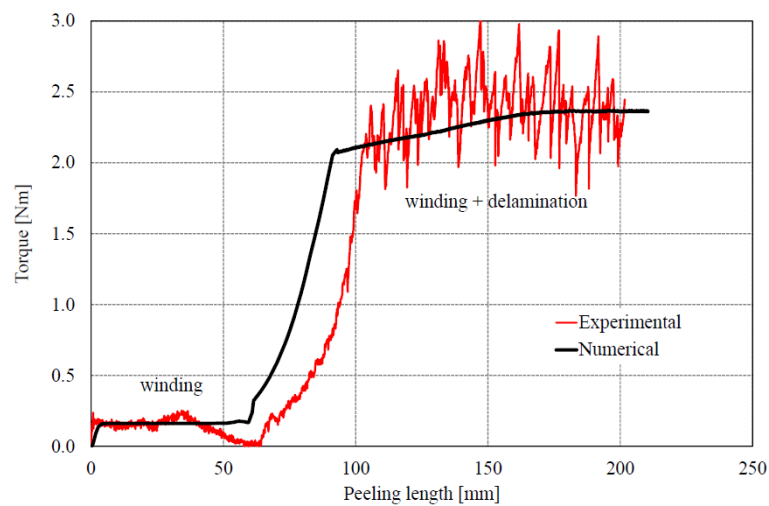
Figure 10: Numerical and experimental results obtained using the new Horizontal Drum Peel test for (a) tape and (b) for a fabric.

(tape and fabric, respectively). This means that although a mixed mode appear during both tests G_c values will be very close to G_{Ic} values. Moreover, numerically obtained ψ values (mode mixity measure) on HDP tests are lower than those for CDP tests.
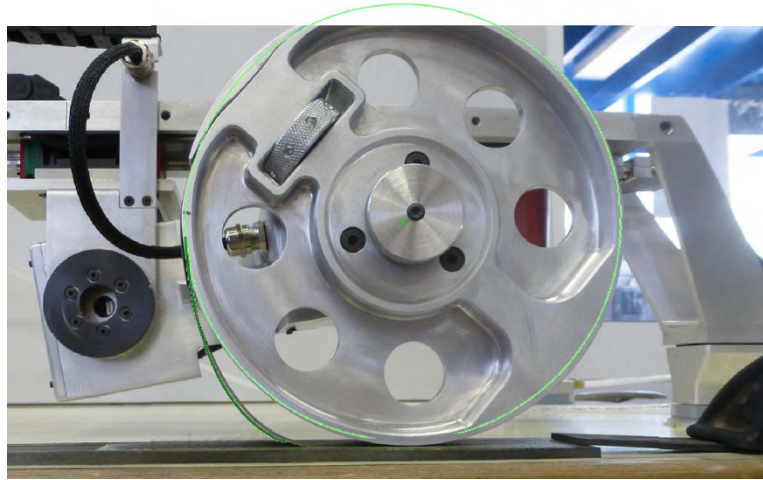
Figure 11: Numerical and experimental deformed shape of the HDP test for a specific moment.

6. Conclusions

The basis for a new in-situ peeling test (HDP) able to determine the interlaminar fracture toughness are set. A test campaign including CDP and the new HDP configuration was developed. Obtained experimental results showed that G_c values obtained using both tests are in very good agreement with each other. Similar results were obtained in the virtual testing (by means of a FEA).

Some characteristics of the HDP test includes: (i) A one step test, leading to obtain T_w and T_d (needed to calculate G_c) easily. (ii) A self-similar crack growth avoiding the necessity to measure the crack length. (iii) A separation of the thin laminate from the drum, tending to its critical radius. Nevertheless, the main advantage of the HDP configuration is the possibility to perform the test "in-situ", without the necessity to extract coupons for their posterior testing in a laboratory.

Some other relevant questions regarding the delamination behaviour on the CDP and HDP tests are analysed. Specifically, this study allowed to

22

confirm that: (i) Crack growth during delamination on CDP and HDP tests are self-similar, i.e. the same pattern is obtained during crack evolution. (ii) A mixed-mode fracture occurs for any coupon (iii) G_c values are very similar to G_{Ic} when the fracture mode mixity angle ψ is lower than 20°, condition that is fulfilled in both cases in the analysed configurations.

Acknowledgements

Appendix A. Delamination mechanisms. Critical moment and critical radius

In this appendix a Finite Element Analysis (FEA) of a simplified problem is presented. The problem includes a specimen with two laminates bonded by an adhesive, see Figure A.11(a). The boundary conditions are a fixed line on the bottom edge of the thick laminate and an applied rotation, θ, at the pre-cracked end of the thin laminate. It is interesting to recall that the imposed rotation causes a constant bending moment (M) and a corresponding constant curvature with radius R, along the thin laminate in the pre-cracked zone.

The FEA was done using the software Abaqus [18]. A 2D FE model including orthotropic properties for the laminates, see Table 3, and geometrically non-linear analysis is considered.
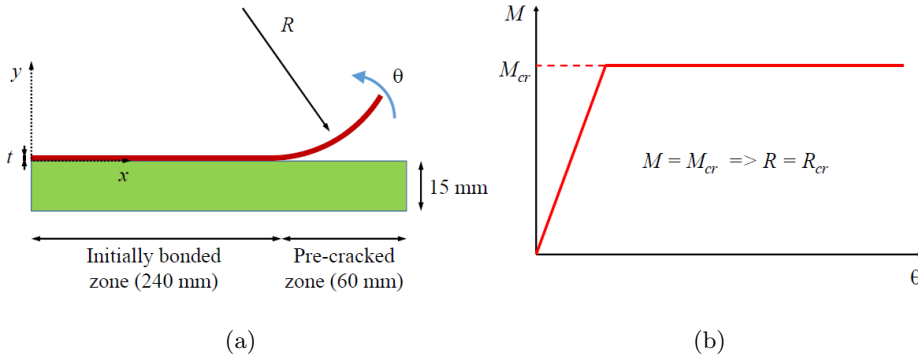
Figure A.12: (a) Simplified model of HDP device and (b) bending moment, M, vs applied rotation, θ, produced in the simplified model.

The bonding configuration is modelled by means of the Abaqus built-in Cohesive Zone Model (CZM) [3], its properties being critical normal traction (σ_c), critical shear traction (τ_c), fracture toughness in mode I (G_{Ic}), fracture toughness in mode II (G_{IIc}) and the biaxility parameter of the Benzeggagh-Kennane criterion (η) [19] shown in Table 4. It is interesting to recall that although both configurations include the same adhesive (FM 300.K05), they have different fracture toughness values. This is due to the fact that the bonding characteristics depend on the adhesive but also on the adherents. The characteristics of bonding configuration 1 represents the FM 300.K05 adhesive joined to a unidirectional laminate while bonding configuration 2 represents the same adhesive joined to a woven fabric. Stiffness parameters needed for the CZM formulation ($K_{nn} = 41861.54$ MPa/mm and $K_{ss} = 6976.92$ MPa/mm) are obtained considering the equations presented in [22] and the following adhesive properties: shear modulus, $\mu = 2.54$ GPa [23] and Poisson ratio, $\nu = 0.4$ [24].

Thicknesses of the thick laminate, adhesive layer and thin laminate are 15 mm, 0.1mm and t (three values are used 0.5, 0.75 and 1mm), respectively. The numerical model includes conforming meshes between the different parts, element length being 0.5mm. Thick laminate elements are 1 mm

24

in thickness (15 elements through the thickness), cohesive elements along the interface are 0.1 mm in thickness (1 element over the thickness), and the thin laminate has 3 elements through its thickness.

Table A.5: M_c values obtained for the different studied configurations in Nm.

Laminate	Interface	t=0.5 mm	t=0.75 mm	t=1 mm
Unidirectional 1, $E_{xx} = 182GPa$	BC1	1.23	2.27	3.52
Unidirectional 2, $E_{xx} = 135GPa$	BC1	1.06	1.96	3.03
Woven fabric [0/90], $E_{xx} = 66GPa$	BC2	0.89	1.65	2.56
Woven fabric [+45/-45], $E_{xx} = 182GPa$	BC2	0.44	0.82	1.26

Numerical results showed that the bending moment, M, initially increased linearly with the applied rotation, θ, and it reaches a critical value, M_c, when the delamination starts, see Figure 10(b). It is interesting to notice that M value keeps constant ($M = M_c$) during the crack propagation. M_c values obtained by the FEAs for the different studied configurations are shown in Table A.5. It can be clearly seen from these results that the M_c value is function of the bonding configuration properties as well as the thin laminate stiffness, i.e. function of the longitudinal stiffness, E_{xx}, and the section moment of inertia, I, which is directly related to the thickness, t; leading to an M_c increase for larger values of E_{xx} and t.

Each M_c value is associated to a critical curvature, $1/R_c$. The critical radius, R_c, can be measured from the numerical results, nevertheless a preliminary R_c value can also be estimated using basic bending beam theory relations:

$$R_c = \frac{(E_{xx}I)}{M_c}, \tag{A.1}$$

R_c values obtained numerically and using (A.1) are presented in Table A.6. Similarly to M_c, R_c values increase for larger values of E_{xx} and t. It is also interesting to notice that results obtained using (A.1) represent a good

25

initial approximation.

Table A.6: R_c values obtained for the different studied configurations in mm.

Laminate	Interface	Solution	t=0.5 mm	t=0.75 mm	t=1 mm
Unidirectional 1	BC1	FEA	38.50	70.24	107.45
Unidirectional 1	BC1	(A.1)	38.61	70.40	107.65
Unidirectional 2	BC1	FEA	33.09	60.60	92.53
Unidirectional 2	BC1	(A.1)	33.20	60.59	92.68
Woven fabric [0/90]	BC2	FEA	18.83	34.81	54.01
Woven fabric [0/90]	BC2	(A.1)	19.24	35.14	53.80
Woven fabric [+45/-45]	BC2	FEA	9.22	19.11	25.75
Woven fabric [+45/-45]	BC2	(A.1)	9.32	17.12	26.28

Appendix B. Fracture mode mixity during delamination

An open question regarding CDP and HDP is the actual fracture mode that occurs during delamination. An established way to measure the fracture mode mixity is by means of the energy-based mixity angle ψ [22, 25], defined by:

$$\tan^2 \psi = \frac{G_{II}}{G_I}, \tag{B.1}$$

where, $\psi = 0°$ represents a pure fracture mode I and $\psi = 90°$ represents fracture in pure mode II.

For CZMs no singularity appears and the ERR mode decomposition (once the fracture process zone is fully developed) are found by integrating over the cohesive surfaces [21]:

$$G_I = \int_{\Gamma_{coh}} t_N \frac{\partial \delta_N}{\partial x} ds, \quad G_{II} = \int_{\Gamma_{coh}} t_S \frac{\partial \delta_S}{\partial x} ds, \tag{B.2}$$

where t_N , t_S , δ_N and δ_S are the normal and shear cohesive tractions and opening displacements respectively. Notice that, integrations in (B.2) have

to be performed over the top or the bottom surface only (but not both).

Table B.7: ψ values obtained for the different studied configurations in degrees.

Laminate	Interface	t=0.5 mm	t=0.75 mm	t=1 mm
Unidirectional 1	BC1	8.96°	9.80°	10.50°
Unidirectional 2	BC1	9.52°	10.29°	11.07°
Woven fabric [0/90]	BC2	10.19°	10.93°	11.71°
Woven fabric [+45/-45]	BC2	14.35°	14.50°	15.29°

In Table B.7, ψ values obtained along the process zone of the cohesive elements for the different studied cases presented in Appendix A. Results showed that the fracture mode mixity seems to be more affected by the laminate material properties of the thin laminate rather than by its thickness. Moreover, $\psi < 16°$ is obtained for every studied configuration. It is interesting to note the influence of the adhesive layer in ψ values obtained in the debonding process, $\psi \approx 38°$ values were obtained in [12] when no adhesive is between the laminates, i.e. modelling a perfect interface.

It is important to note that ψ values larger than $45°$ not necessarily implies G_c values closer to G_{IIc}. This is due to the way G_c evolves for different ψ values. In Figure B.13, usual G_c evolutions (for $G_{IIc} = 2G_{Ic}$) based on the Hutchinson and Suo phenomenological law [25] and the Benzeggagh and Kenane criterion [19] are shown.

Studied evolutions of G_c on Figure B.13 show that for $\psi < 20°$, although a fracture mode mixity appears, $G_c \cong G_{Ic}$. This results are in line with previous experimental data obtained in literature [11], where CDP values were very close to those obtained by DCB tests (pure mode I, G_{Ic}).

Appendix C. Maximum bending stresses on the thin laminate

A simplified parametric study has been developed using a pure bending beam with the aim to select an admisible range of laminate thickness. Using
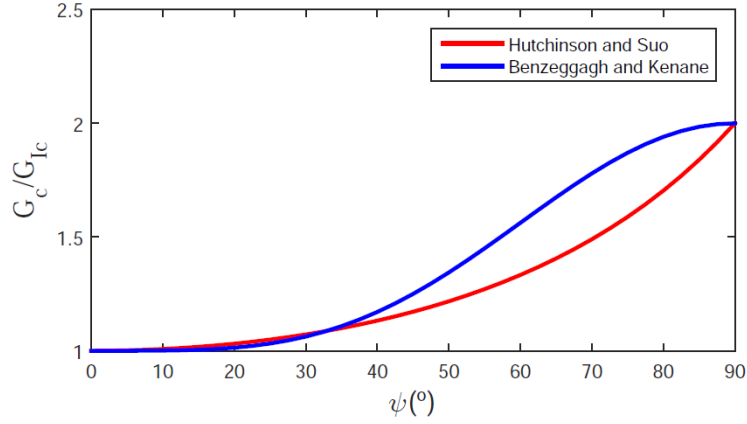
27

Figure B.13: G_c evolution in function of ψ based on the Hutchinson and Suo phenomenological law [25] and the Benzeggagh and Kenane criterion [19] for $G_{IIc} = 2G_{Ic}$.

the classical bending beam theory, σ values can be approximated by:

$$\sigma = \frac{E_{xx}t}{2R_c}, \tag{C.1}$$

Three variables were used in this study: joint toughness, G_c, thickness, t, and longitudinal stiffness, E_{xx}, of the thin laminate; R_c being computed by (A.1).

Table C.8, shows the maximum stress, σ, and critical radius, R_c, obtained for several combinations of G_c, t and E_{xx}. Typical configurations are remarked in bold.

Admissible σ values obtained in a 3 point bending test (by a test campaign) for ± 45 woven fabric (E_{xx}=15.9 GPa) and unidirectional tape (E_{xx}=182 GPa) are 350 and 1200 MPa, respectively. Then, a range of thicknesses can be determined in order to asure that delamination is produced prior to the breakage of the thin laminate caused by an extreme bending. Thus, for the fabric case an adequate laminate thickness could be between 0.75 and 1 mm. While, for the tape case the thickness could be between 0.5 and 1 mm.

Table C.8: Maximum bending stresses, obtained by (B.2), for several configurations.

G_c (Jm^{-2})	E_{xx} (GPa)	15.9			182		
	t (mm)	0.5	0.75	1.0	0.5	0.75	1.0
300	R_c (mm)	16.61	30.52	46.49	56.21	103.27	158.99
	σ (MPa)	239.25	195.35	169.17	809.44	660.91	572.36
600	R_c (mm)	11.75	21.58	33.23	**39.75**	**73.02**	**112.42**
	σ (MPa)	338.35	276.26	239.25	**1144.73**	**934.67**	**809.44**
900	R_c (mm)	**9.59**	**17.62**	**27.13**	32.45	59.62	91.79
	σ (MPa)	**414.39**	**338.35**	**293.02**	1402.00	1144.73	991.36
1200	R_c (mm)	8.31	15.26	23.50	28.11	51.63	79.49
	σ (MPa)	478.50	390.69	338.35	1618.89	1321.82	1144.73

On the other hand, recalling that $R_D > R_c$ will enable a self-similar crack propagation, $R_D \gtrsim 90$ mm values seem to be adequate for a large range of E_{xx} and t values, Finally, $R_D = 95$ mm is chosen to be used in the HDP prototype.

References

[1] P.P. Camanho, A. Fink, A. Obst, S. Pimenta. Hybrid titanium-CFRP laminates for high-performance bolted joints. Composites Part A 40:12 (2009) 1826–1837.

[2] C. Stocchi, P. Robinson, S.T. Pinho. A detailed finite element investigation composite bolted joints with countersunk fasteners. Composites Part A 52 (2013) 143–150.

[3] J. Reinoso, A. Blázquez, L. Távara, F. París, C. Arellano (2016) Damage tolerance of composite runout panels under tensile loading. Composites Part B, 96 (2016) 79–93.

[4] Airbus, AITM 1-0005. Fibre reinforced plastics - Determination of interlaminar fracture toughness energy - Mode I - G1c.

[5] Airbus, AITM 1-0053. Carbon fiber reinforced plastics. Determination of fracture toughness energy of bonded joints. Mode I. GIC test.

[6] ISO, ISO 15024. Fibre-reinforced plastic composites-determination of mode I interlaminar fracture toughness, GIc, for unidirectionally reinforced materials.

[7] ASTM-D5528. Standard Test Method for Mode I Interlaminar Fracture Toughness of Unidirectional Fiber-Reinforced Polymer Matrix Composites.

[8] A. Szekrényes J. Uj. Advanced beam model for fiber-bridging in unidirectional composite double-cantilever beam specimens. Engineering Fracture Mechanics 72 (2005) 2686–2702.

[9] J. Jumel, M K. Budzik, M.E.R. Shanahan. Beam on elastic foundation with anticlastic curvature: Application to analysis of mode I fracture tests. Engineering Fracture Mechanics. 78 (2011) 3253–3269.

[10] ASTM-D1781. Standard test method for climbing drum peel for adhesives.

[11] F. Daghia, C. Cluzel. The Climbing Drum peel Test: An alternative to the Double Cantilever Beam for the determination of fracture toughness of monolithic laminates. Composites Part A. 78 (2015) 70-83.

[12] M. D. Thouless, H. M. Jensen. Elastic Fracture Mechanics of the Peel-Test Geometry. The Journal of Adhesion. 38:3-4 (1992) 185-197.

[13] W.J.B. Grouve, L.L. Warnet, R. Akkerman. Critical assessment of the mandrel peel test for fiber reinforced thermoplastic laminates. Engineering Fracture Mechanics 101 (2013) 96–108.

[14] V. Pavelko, K. Lapsa, P. Pavlovskis. Determination of the mode I inter-laminar fracture toughness by using a nonlinear double-cantilever beam speci- men. Mechanics of Composite Materials 52:3 (2016)347-358.

[15] L. Távara, V. Mantič, E. Graciani, J. Cañas, F. París . Analysis of a Crack in a Thin Adhesive Layer between Orthotropic Materials: An Application to Composite Interlaminar Fracture Toughness Test. Computer Modelling in Engineering and Science 58 (2010) 247-270.

[16] V. Mollón, J. Bonhomme, J. Viña, A. Argüelles. Mixed mode fracture toughness: An empirical formulation for GI /GII determination in asymmetric DCB specimens. Engineering Structures 32 (2010) 3699-3703.

[17] J. Cañas, F. París, L. Távara, A. Blázquez, A. Estefani, G. Santacruz, T. Stöven. P201830349. Equipo de ensayo para la determinación in situ de la tenacidad a la fractura de uniones encoladas. (2018).

[18] Abaqus-Inc. Abaqus user manual, Version 6.14. Providence, RI, USA: Dassault Systems Simulia Corp. (2014).

[19] M.L. Benzeggagh, M. Kenane. Measurement of mixed-mode delamina-tion fracture toughness of unidirectional glass/epoxy composites with mixedmode bending apparatus. Composite Science and Technology 56:4 (1996) 439–49.

[20] K. M. Liechti, T. Freda. On the use of laminated beams for the de-termination of pure and mixed-mode fracture properties of structural adhesives. The Journal of Adhesion, 28 (1989) 145-169.

[21] M. Conroy, A.J. Kinloch, J.G. Williams, A. Ivankovic. Mixed mode partitioning of beam-like geometries: A damage dependent solution. Engineering Fracture Mechanics 149 (2015) 351–367.

[22] V. Mantič, L. Távara, A. Blázquez, E. Graciani, F. París. A linear elastic - brittle interface model: Application to the onset and propagation of a fibre- matrix interface crack under biaxial transverse loads, International Journal of Fracture 195 (2015) 15-38.

[23] Cytec. FM $^{\circledR}$ 300 Epoxy Film Adhesive. Technical Data Sheet. Tempe, Arizona, USA: Cytec Industries Inc. (2013).

[24] W.S. Johnson, S. Mall. A fracture mechanics approach for designing adhesively bonded joints. In: Delamination and Debonding of Materials (Eds. W.S. Johnson). (1985) 189–199.

[25] J.W. Hutchinson, Z. Suo. Mixed mode cracking in layered materials. Advances in Applied Mechanics 29 (1992) 63–191.